ACS NANO
Cite This: ACS Nano 2018, 12, 4702−4711
www.acsnano.org

Memristive Ion Channel-Doped Biomembranes as Synaptic Mimics

Joseph S. Najem,[†,#] Graham J. Taylor,[‡,#] Ryan J. Weiss,[§] Md Sakib Hasan,[§] Garrett Rose,[§] Catherine D. Schuman,[∥] Alex Belianinov,[⊥] C. Patrick Collier,[*,⊥] and Stephen A. Sarles[*,#]

[†]Joint Institute for Biological Sciences, Oak Ridge National Laboratory, Oak Ridge, Tennessee 37831, United States
[‡]Bredesen Center for Interdisciplinary Research, University of Tennessee, Knoxville, Tennessee 37996, United States
[§]Department of Electrical Engineering and Computer Science, University of Tennessee, Knoxville, Tennessee 37916, United States
[∥]Computer Science and Mathematics Division, Oak Ridge National Laboratory, Oak Ridge, Tennessee 37831, United States
[⊥]Center for Nanophase Materials Sciences, Oak Ridge National Laboratory, Oak Ridge, Tennessee 37831, United States
[#]Department of Mechanical, Aerospace and Biomedical Engineering, University of Tennessee, Knoxville, Tennessee 37916, United States

Supporting Information

ABSTRACT: Solid-state neuromorphic systems based on transistors or memristors have yet to achieve the interconnectivity, performance, and energy efficiency of the brain due to excessive noise, undesirable material properties, and nonbiological switching mechanisms. Here we demonstrate that an alamethicin-doped, synthetic biomembrane exhibits memristive behavior, emulates key synaptic functions including paired-pulse facilitation and depression, and enables learning and computing. Unlike state-of-the-art devices, our two-terminal, biomolecular memristor features similar structure (biomembrane), switching mechanism (ion channels), and ionic transport modality as biological synapses while operating at considerably lower power. The reversible and volatile voltage-driven insertion of alamethicin peptides into an insulating lipid bilayer creates conductive pathways that exhibit pinched current−voltage hysteresis at potentials above their insertion threshold. Moreover, the synapse-like dynamic properties of the biomolecular memristor allow for simplified learning circuit implementations. Low-power memristive devices based on stimuli-responsive biomolecules represent a major advance toward implementation of full synaptic functionality in neuromorphic hardware.

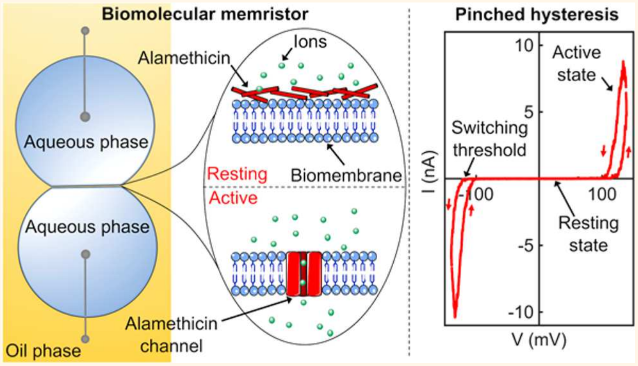

KEYWORDS: *biomolecular memristor, alamethicin, memristor, ion channel, biomembrane, neuromorphic computing, lipid bilayer*

Despite major progress in very-large-scale-integration (VLSI) circuits,[1−4] neuromorphic networks to date have failed to achieve the neuronal density, power efficiency, and complexity of the human brain. Unlike current solid-state technology, the brain leverages sophisticated molecular mechanisms to continually reconfigure connectivity between neurons.[5,6] Synaptic plasticity[5] enables the brain to remember patterns and adapt to incoming information, perform parallel operations at immense scale, and operate at exceptionally high efficiencies (∼20 W).[7]

VLSI networks emulate synaptic activities *via* three-terminal transistors that bear little phenomenological similarity to biosynapses[8,9] and rely on expensive, power-hungry complementary metal-oxide−semiconductor circuitry. Alternatively, two-terminal memory-resistive elements (memristors) have been developed[10−15] to mimic synapse plasticity and require less power.[16] A memristor can reconfigure its resistance (*synaptic weight*) based on electrical activity of connected "neurons"; this plasticity allows memory and computing to be colocated as in biosynapses. The functionality offered by a single memristor can be used to replace up to 10 transistors on a chip,[16] which makes them ideal for data storage, neuromorphic applications, and large-scale integration.[11]

Ion drift memristors,[10,17,18] the most characterized examples of solid-state memristors, offer variable resistance readouts over large dynamic ranges. Yet their nonvolatility, fast resistive

Received: February 16, 2018
Accepted: March 26, 2018
Published: March 26, 2018

DOI: 10.1021/acsnano.8b01282

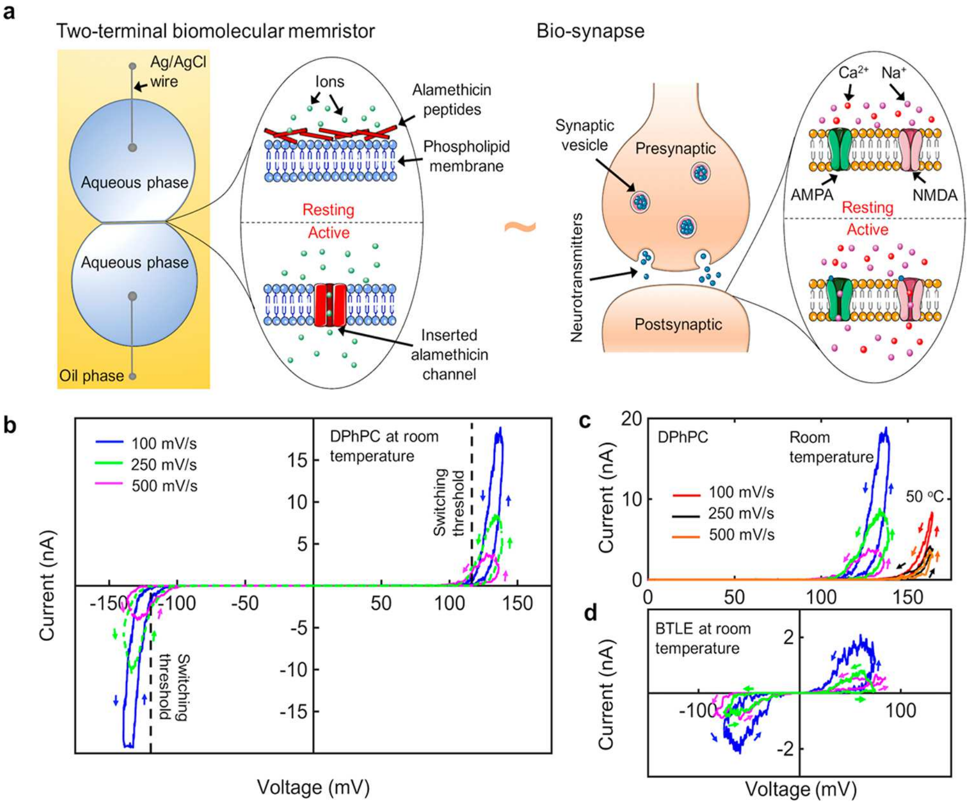

Figure 1. Two-terminal biomolecular memristors that mimic the structure and switching mechanism of biosynapses and exhibit nonlinear memristive behavior as well as bipolar threshold switching. (a) Illustration of the biomolecular memristor (left) *versus* an actual biosynapse (right). In biosynapses, an action potential traversing the presynaptic neuron causes voltage-gated calcium channels to open, causing an influx of Ca^{2+} ions. Upon binding with Ca^{2+} ions, neurotransmitter (NT)-loaded synaptic vesicles dock to the presynaptic plasma membrane and fuse to release NTs into the synaptic cleft. The released NTs are received at the postsynaptic plasma membrane by AMPA and NMDA receptors/ions channels, events that trigger ion flux into the postsynaptic neuron that depolarizes the cell.[47] Importantly, these channels remain closed, holding the membrane in an insulating state, until NTs bind to their receptors, at which point the conductance of postsynaptic membrane increases exponentially. A lipid bilayer formed at the interface of lipid-coated water droplets establishes a two-terminal biomolecular memristor that mimics the structure and composition of the synaptic plasma membranes. This embodiment of a biomolecular memristor also includes alm ion channels for voltage-controlled signal transmission, imitating the switching mechanisms of synapses. Representative nonlinear threshold switching *I*−*V* relationships measured at three different voltage sweep rates as shown for (b) a DPhPC-memristor at room temperature and (c) DPhPC devices at two temperatures. For comparison, we used only positive voltages and found that the switching threshold increased as the oil temperature increased to 50 °C. (d) BTLE-based memristor at room temperature. All devices were constructed with droplets containing 1 μM alm.

switching, rigidity, and electronic operation make them biologically unrealistic. These features of first-generation devices resulted in an inability to exhibit spike-timing-dependent plasticity, an important aspect of learning that was only recently emulated by second-generation ion drift memristors.[19,20] More recently, researchers developed an inorganic diffusive memristor[21,22] that closely emulated synaptic Ca^{2+} dynamics. This approach yielded more biologically realistic memristors and, consequently, fully memristive neural networks capable of unsupervised learning.[22]

Low-cost, low-power, and biocompatible organic polymeric memristive devices have also been developed,[23−25] but they suffer from low resistance ratios, slow kinetics of ion diffusion through the conductive polymer, and poor switching stability. Other reported synthetic memristors include ferroelectric,[26,27] manganite,[28,29] and spintronic[30] varieties.

A key takeaway is that the behaviors of synthetic memristors are largely phenomenological; they bear no resemblance to the structure, composition, or switching mechanisms of biosynapses. Existing memristors emulate a handful of simple synaptic functions, bypassing many others and ignoring the actual mechanisms governing synaptic functionality. To solve the exponentially increasing computing demands, avoid Moore's law and Dennard scaling,[31] and enable efficient as well as intelligent edge computing,[32] a more faithful synaptic model should target not only the integration density and computational power efficiency of current approaches but also the degree of biological realism on both structural and functional levels. This approach requires designing systems that are energy efficient, soft, stochastic, fault tolerant, capable of self- or external-healing, and preferably biological.

Here we report a biomolecular memristor with composition, structure, switching mechanism, and ionic transport similar to biosynapses. The two-terminal device consists of a highly insulating (~10 GΩ),[33] 3−5 nm thick planar lipid bilayer (Figure 1a) assembled at the interface of lipid-encased aqueous droplets held in an oil reservoir[34] (Methods and Supplementary Figure S1). Conductive and memristive ion channels were realized through reversible, voltage-driven insertion of alamethicin[35] peptides (alm) into the insulating bilayer membrane (Supplementary Figure S2). We demonstrate the memristive nature of the device experimentally *via* pinched

Table 1. Time and Switching Characteristics of the Biomolecular Memristor for Different Lipid Types and Temperatures

lipid type	temperature	$V_{threshold}$ (mV)	τ_r (ms)	τ_p (ms)	τ_d (ms)
DPhPC	RT	120	6.8 ± 1.2	99.5 ± 17.7	1 ± 1.3
DPhPC	50 °C	150	3.7 ± 0.5	75.1 ± 11.1	8.55 ± 2.74
BTLE	RT	25	100 ± 37	420 ± 61.2	23.3 ± 6.11

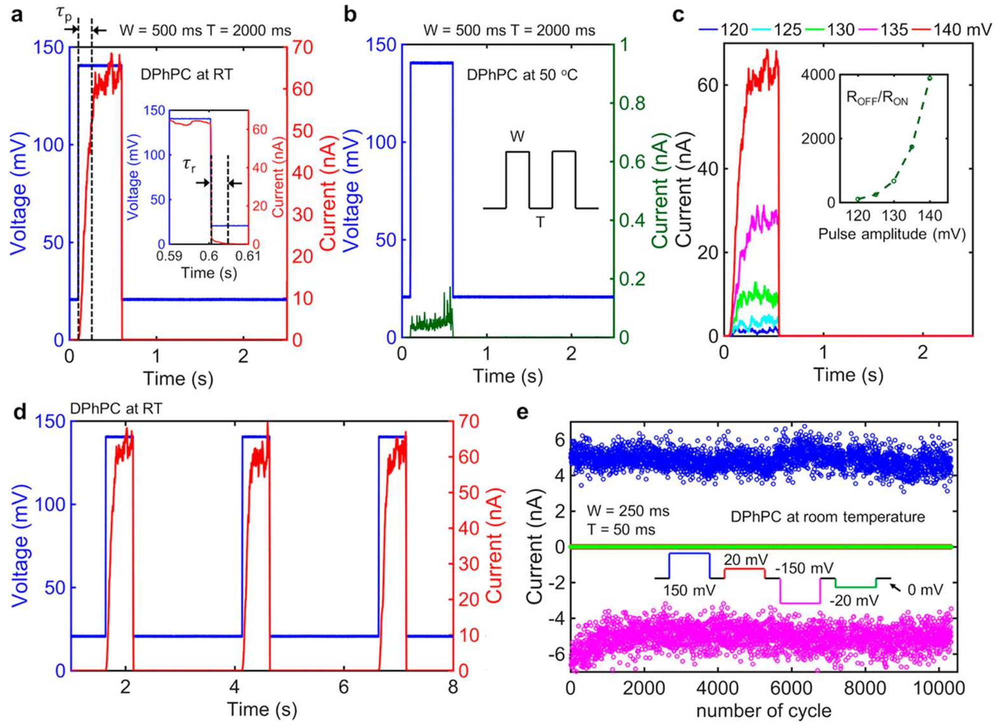

Figure 2. Time characteristics and endurance of the biomolecular memristor in response to above-threshold switching pulses. (a) The DPhPC-based device at room temperature switched from an insulating state (OFF) to a low-resistance state (ON) in response to a switching pulse greater than $V_{threshold}$ (140 mV). The response exhibited a delay time of ~1 ms and potentiation time constant of ~100 ms. When the voltage was lowered to a subthreshold level, the device switched back to an insulating state with a relaxation time constant (τ_r, described in the inset) of ~7 ms. (b) Switching behavior of the DPhPC-based memristor at 50 °C. Similar switching dynamics were observed; however the amplitude of the current in the ON-state was significantly lower, due to a higher $V_{threshold}$. The inset describes the pulses that we used to characterize our devices, where W is the width of the pulse (ON-time) and T is the duration between consecutive pulses (OFF-time). (c) Nonlinear current response of the device described in (a) to multiple pulses with different amplitudes. The inset shows the resistance ratios between the OFF- and ON-states (R_{OFF}/R_{ON}) corresponding to each of the switching pulses. (d) Repeatable and consistent switching of the device described in (a) in response to a pulse wave. (e) Bipolar endurance-cycling test of the device for more than 10 000 cycles at room temperature. The inset describes one cycle of the pulse wave used in this experiment.

hysteresis[36] in the current−voltage (I−V) plane and theoretically through modeling. We find the inherent active properties of this biomolecular memristor are analogous to those of ion channels[37] in pre- and postsynaptic neurons that are partially responsible for short-term and long-term plasticity. We verify this similarity by demonstrating paired-pulse facilitation (PPF) and depression (PPD),[38] which have previously required sophisticated materials and fabrication processes to be achieved in conventional solid-state memristors or other devices.[21,39] Additionally, we showcase *via* simulation evidence of short-term learning and, when paired with a nonvolatile metal-oxide memristor, spike-timing-dependent plasticity (STDP).[6] Due to the ionic nature and low switching voltages (millivolts), all computing operations occur at power consumption levels (pico- to nanowatts) orders of magnitude lower than most solid-state memristors (microwatts).[40]

RESULTS AND DISCUSSION

Two-Terminal, Biomimetic Memristor. In this study, we reconstituted alm peptides into biomimetic membranes assembled from two types of lipids: (i) diphytanoylphosphatidylcholine (DPhPC), a synthetic lipid known for its chemical stability and low ion permeability,[41] and (ii) porcine brain total lipid extracts (BTLE), a mixture that resembles the composition of human synapse membranes.[42] Unlike state-of-the-art memristors, which require expensive and sophisticated fabrication methods and materials, planar lipid membranes spontaneously self-assemble upon contact between lipid-encased aqueous droplets due to the entropically driven exclusion of oil[43] and are inexpensive. At low transmembrane voltages, where alm peptides are surface-bound (*i.e.*, the *resting state*), the biomembrane was highly resistive to ion transport. However, the device abruptly switched into a voltage-dependent conductive (*active*) state at voltages exceeding a certain bias ($V_{threshold}$), which varied by lipid type and temperature (Table 1). Above $V_{threshold}$, alm peptides inserted into the membrane and self-organized to create transmembrane channels capable of ion transport. As illustrated in Figure 1a, this scheme resembles the voltage-modulated variable conductance of a biosynapse. The typical interface diameter (~250

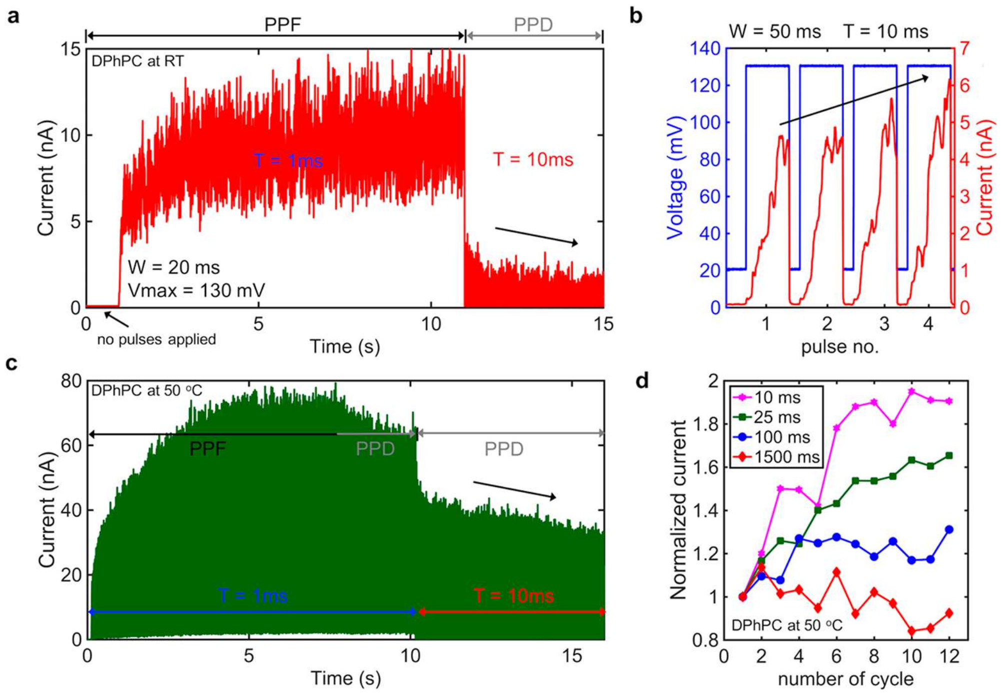

Figure 3. Short-term synaptic plasticity of the biomolecular memristor. (a) Demonstration of short-term synaptic plasticity PPF and PPD behaviors of a DPhPC-based memristor at RT. PPF and PPD are forms of short-term plasticity that occur in the presynaptic neuron and are caused by two presynaptic spikes that are evoked in succession.[50] A series of 130 mV pulses with a 20 ms ON-time (W) and applied at variable OFF-times (T) caused either accumulated increases (PPF) or decreases (PPD) in current output. (b) Measured response of a DPhPC-based memristor at RT to a series of 130 mV, 50 ms pulses separated by an OFF-time of 10 ms. (c) Measurements of current *versus* time showing PPF and PPD behaviors for an alm−DPhPC case at 50 °C. (d) Normalized (with respect to the current output from the first pulse) values of RMS current measured for consecutive pulses at various OFF-time values.

μm) of our device was larger than the synaptic active zone (~300 ± 150 nm);[44] however the interface diameter can be reduced by decreasing the size of the droplets to dimensions closer to those of natural synapses.[45]

To demonstrate that an alm-doped membrane is memristive, we measured I−V relationships for multiple lipid types and temperatures in response to triangular voltage waveforms at various sweep rates (Figure 1b, c, and d). For all cases, we observed pinched and symmetric hysteretic I−V loops, highlighting the memristive behavior of the device as defined by Chua *et al.*[36] The system exhibited bipolar switching due to alm inserting from both sides of the membrane, with net conductance defined by the total number of alm channels. For comparison, alm-free membranes were highly insulating and exhibited far smaller changes in conductance at voltages less than ±150 mV (Supplementary Figure S3).

Adjusting temperatures or membrane composition enabled precise control of these alm-mediated responses. For example, increasing the temperature of a DPhPC membrane to 50 °C raised $V_{\text{threshold}}$ (Table 1), likely due to increasing the oil content of the membrane,[46] but reduced the I−V hysteresis. Separately, replacing DPhPC with BTLE lipids lowered $V_{\text{threshold}}$ and increased hysteresis. These data also showed that I−V hysteresis is dependent on the voltage sweep rate (V_r), which is a quality of generic memristors.[36]

Switching Characteristics. We characterized the dynamic switching behavior of our biomolecular memristors in response to stepwise voltage pulses. An alm−DPhPC memristor at room temperature (RT) responded to a 500 ms, 140 mV switching pulse with an exponential increase in current corresponding to the insertion of alm peptides and formation of pores ($R_{\text{ON}} \approx$ 2.5 MΩ). This increase in current exhibited a delay (t_d) of 1 ms and potentiation time constant (τ_p) of ~100 ms. The device returned to an insulating state ($R_{\text{OFF}} \approx$ 10 GΩ), with a relaxation time constant (τ_r) of ~7 ms when the voltage dropped to 20 mV ($<V_{\text{threshold}}$). At 50 °C, the same switching pulse resulted in lower current output ($R_{\text{ON}} \approx$ 1.5 GΩ), suggesting that fewer alm pores formed within the membrane, which was consistent with the results displayed in Figure 1c. We observed a smaller relaxation time constant, τ_r, in this case (~3 ms), due to the oil-rich membrane, which created unfavorable conditions for alm incorporation.[46] We also performed these measurements on an alm−BTLE memristor at room temperature (Supplementary Figure S4), where significantly slower switching dynamics were observed. Table 1 summarizes the switching dynamics and relaxation time constants obtained for all three cases. Note that the channel decay rate (especially in the BTLE case) is similar to values of N-methyl-D-aspartate (NMDA) receptor relaxation rates observed in biosynapses, which usually lasts for milliseconds.[48]

In Figure 2c, we confirm that both the steady-state current during the ON-state and the OFF/ON resistance ratios grew exponentially with the amplitude of the switching pulse ($100 < R_{\text{OFF}}/R_{\text{ON}} < 4000$ for alm−DPhPC at RT). Conductance changes of alm-based memristors can be tuned independently with peptide and salt concentrations, as well as lipid type and temperature, allowing for significant flexibility in optimizing resistance ratios ($R_{\text{OFF}}/R_{\text{ON}}$). For example, by extrapolating the I−V responses shown in Figure 1d, we predict that ±180 mV switching pulses would yield resistance ratios as high as 50 000 in alm−BTLE devices, values similar to those of biological synapses.[49]

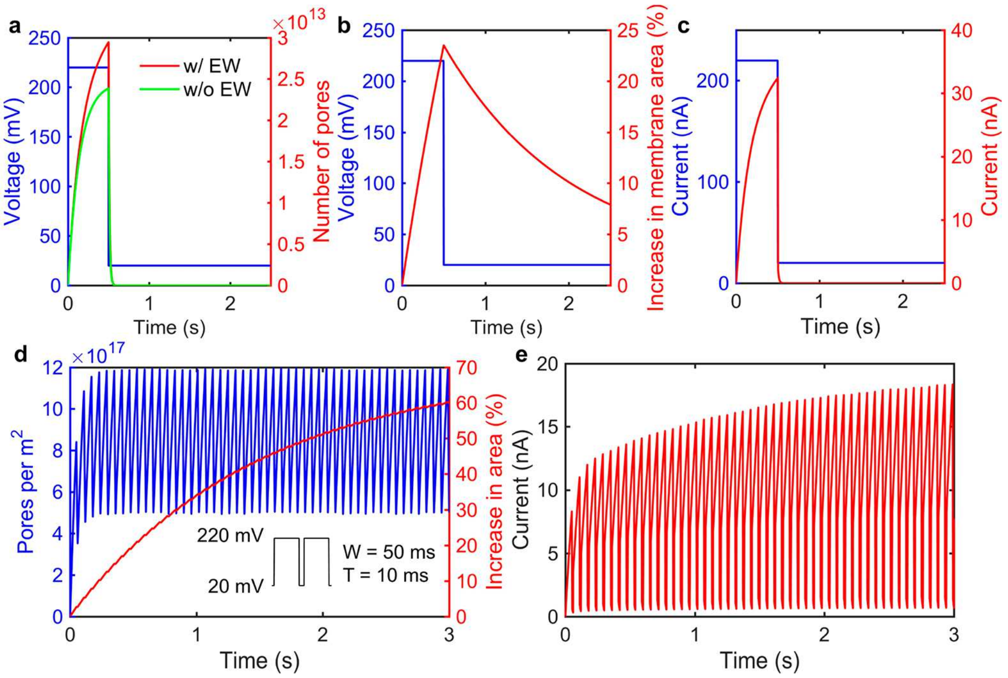

Figure 4. Simulated response of the biomolecular memristor. (a) Simulation showing the increase in number of alm pores (red) in response to a voltage pulse (220 mV, *W* = 500 ms, *T* = 2000 ms). For the results displayed in green, we considered that the system did not exhibit any EW. (b) Percentage increase in lipid membrane area in response to the same voltage pulse. (c) Simulation showing the current output of the device due to the combined effect of pore formation and EW in response to the same voltage pulse. (d and e) Simulations dissecting the role each phenomenon plays in generating the PPF behavior. (d) The number of pores per area reached steady state in ~100 ms, while the area increase occurred over a period of several seconds in response to a pulse wave (described in inset). (e) Corresponding current response demonstrates PPF-like behavior observed in experiments. All simulations were based on parameters for alm−DPhPC at room temperature (Tables 1, S1, S4).

These switching characteristics were consistent from one cycle to another when the OFF-time between unipolar switching pulses was sufficiently long (2 s) (Figure 2d). We also demonstrated repeatable switching and reading currents for at least 10 000 cycles of bipolar pulses, shown in Figure 2e. In addition to showcasing the switching durability, these two tests highlight that surface-bound alamethicin present on one or both sides of the membrane can be independently activated. In the former, a positive, unipolar voltage inserts only alamethicin peptides present on the positive electrode side of the membrane. In the latter, alternating voltages at opposite polarities drive the insertion of separate populations of alamethicin peptides residing on opposite sides of the membrane.

Short-Term Facilitation and Depression. In contrast to long OFF-times, we discovered that switching pulses separated by shorter OFF-times caused the biomolecular memristors to accumulate changes in conductance, which emulated PPF and PPD in biosynapses.[50] Figure 3a shows the response of an alm−DPhPC memristor at RT to a 130 mV, 20 ms pulse wave with 1 ms OFF-time for the first 10 s, and 10 ms for the remaining cycles. At 1 ms between pulses, the peak current increased with successive pulses until reaching a steady state, emulating PPF. During subsequent pulses separated by 10 ms, we observed that the instantaneous current between pulses approached zero, while the peak current gradually reduced, emulating PPD. PPF-like accumulation of current also occurred at OFF-times of 10 ms (W = 50 ms) (Figure 3b), despite the instantaneous current returning to zero between pulses, when pulses with shorter OFF-times were not applied beforehand. Moreover, we measured PPF and PPD in alm−DPhPC memristors at 50 °C (Figure 3c,d) and alm−BTLE memristors at RT (Supplementary Figure S5) for varying OFF-times. However, unlike alm−DPhPC at RT, a continuous series of pulses with 1 ms OFF-times resulted in a nonmonotonic rise in peak current for alm−DPhPC at 50 °C (Figure 3c). This is analogous to PPF followed by PPD that can occur in biosynapses due to excessive stimulation.

Physical Mechanisms and Simulations. Two phenomena can occur when voltage (V) is applied to a droplet-based bilayer containing alm: (1) surface-bound alm peptides insert and aggregate to form conductive pores, and (2) the area of the bilayer increases due to electrowetting (EW),[34] providing more space for alm insertion. These phenomena together drive an exponential increase in the total number of open channels, N, in the membrane, which creates an exponential increase in current, I. Thus, we write the I−V relationship for our biomolecular memristor as

$$I = G(N_a, A_m)V \tag{1}$$

Here, G is the nominal conductance, which is dependent on two state variables: the number of alamethicin pores per unit area, N_a, and the fractional change in membrane area, A_m, due to EW. The dynamic state equation for N_a is given by

$$\frac{dN_a}{dt} = \frac{1}{\tau_0 e^{V/V_\tau}}(N_0 e^{(V/V_e)} - N_a) \tag{2}$$

where τ_0, V_τ, N_0, and V_e represent the time constant for pore closure, τ, at zero volts, the voltage required to drive an e-fold increase in τ, a proportionality constant related to the number

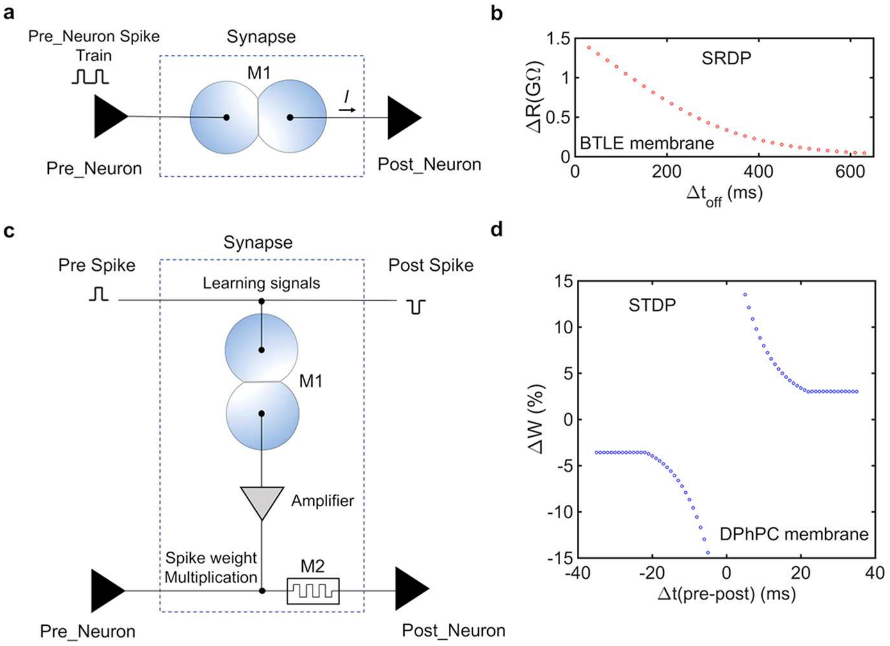

Figure 5. Online learning circuit application. (a) A biomolecular memristor (M1) placed as a synapse between a neuron facilitated short-term learning and updated its weight by continued activation in a relative time span. The current output from M1 into the post-neuron increased as the pre-neuron produced voltage spikes closer together in time. (b) Resulting weight change of the synapse connection facilitated by M1. The plot shows the change in output current of M1 recorded at the second pre-neuron spike in succession. Different time intervals between pre-neuron spikes resulted in different output currents for the post-neuron to accumulate. For these simulations, the parameters for alm in a BTLE membrane were used, since its slower dynamics were favorable for this implementation. (c) Circuit setup using M1 to facilitate STDP. M1 works in conjunction with a nonvolatile memory device (M2) to update weight values. Flow control of the inputs into the STDP circuitry uses two diodes and three switches. The diodes direct the pre-spike and inverted post-spike through the device. Assuming the spikes do not overlap, the pre- and post-spikes activate M1 and produce different output currents based on the time difference between the spikes. While it is possible M1 and M2 could be directly wired in series, a trans-impedance amplifier was included to hold M2 at constant voltage on the bottom node to amplify the current output and cause switching in the nonvolatile memristor of any type. (d) Resulting weight changes for long-term learning from ideal component simulations. Weight change was determined by the change in conductance of the nonvolatile memristor (M2). Parameters for a DPhPC membrane at room temperature were used to simulate the STDP results, since faster dynamics are favorable for this implementation.

of open pores at zero volts, and the potential required to increase the number of pores *e*-fold.[51]

The state equation describing the fractional change in membrane area, $A_{m,}$ is

$$\frac{dA_m}{dt} = \frac{1}{\tau_{ew}}(\alpha v^2 - A_m(t)) \tag{3}$$

where τ_{ew} and α are the time constant and proportionality constant of EW, respectively.

Therefore, the total memconductance of our voltage-controlled device becomes

$$G(t) = G_u N_a(V_m, t) A_0(1 + A_m(t)) \tag{4}$$

where G_u is the unit conductance for open pores and A_0 is the lipid membrane area at zero volts. A detailed derivation is provided in the Supporting Information. Solving eqs 2 and 3 allows for the total current to be computed *via* eqs 1 and 4. These state equations and our experimental results allow us to characterize our biomolecular device as a "generic memristor".[15,36]

To distinguish the mechanisms that drive memristance and volatility, and to explain PPF- and PPD-like responses, we determined values for the state equation parameters (see Methods, Tables S1−S4). These values enabled accurate predictions *via* our model (see Supplementary Figures S6 and S7) of the $I-V$ behaviors we experimentally observed in Figure 1, and they reveal the source of $I-V$ hysteresis and its rate dependence: the finite kinetics of electrowetting (∼1 s) and alamethicin channel potentiation (∼100 ms) cause the net current to lag the applied voltage. As a result of these sources of lag, N_a and A_m accumulate slowly to produce a larger net current by the time the voltage is decreasing from a maximum value than during the increasing leg of the voltage sweep. This inherent lag time also affects the frequency response of the system, where fewer channels can insert and smaller increases in membrane area can occur as the sweep rate is increased from 100 to 500 mV/s. This mechanism is consistent with our observations of minimal hysteresis for sweep rates slower than 20 mV/s and minimal resistive switching response at frequencies of >5 Hz.

We then simulated dynamic current responses to switching pulses as was performed experimentally for Figure 2. In the first simulation, we applied a single voltage pulse (Figure 4a) and saw that the total number of pores (red) increased exponentially, accompanied by a slight increase in membrane area (∼20%) (Figure 4b). Without EW (simulated by setting $\alpha = 0$), the total number of pores was lower by this same percentage. However, reducing the voltage to less than $V_{threshold}$ resulted in a rapid decay of N to zero (Supplementary Figure S8 confirms the decay rate depends on the subthreshold voltage), whereas the membrane area fell off much more slowly (see also Supplementary Figure S9). The current output due to

DOI: 10.1021/acsnano.8b01282
ACS Nano 2018, 12, 4702−4711

the combined effect of both phenomena is shown in Figure 4c. This response emphasizes that while pore insertion (and relaxation) are much faster than changes in membrane area, the net current through the memristor is still fully dependent on inserted alm channels, which only occurs when $V > V_{\text{threshold}}$. This means that channel dynamics dominate the dynamic response to a single pulse.

However, the dynamics of area growth become important when the OFF-time between pulses shrinks. For example, our simulation shows that the maximum value of N_a (blue) saturated within 2−3 pulses (~100 ms), whereas A_m (red) grew steadily over many seconds (Figure 4d) in response to 220 mV, 50 ms pulses separated by 10 ms delays at 20 mV (see also Supplementary Figure S10a). This means that the dynamics of N are limited by the rate of change in area (Figure 4e) and that accumulation of changes in conductance (either PPF or PPD) can be tuned by the frequency and duty cycle of the switching pulse with respect to the time constants for each membrane (Table 1, Tables S1−S4). The fact that values of τ_p are generally larger than τ_r and that τ_{ew} can be larger for positive *versus* negative changes in A_m (Supplementary Figure S10b) means that PPF occurs when both the peak voltage exceeds $V_{\text{threshold}}$ and the time between pulses is shorter than the relaxation time of the membrane area after EW ($<5\tau_{ew}$). In contrast, PPD can occur at the same pulse amplitude when larger OFF-times cause the area of the membrane to decrease and more channels to close.

These simulations allowed us to conclude that there are two time scales for an alm-doped memristor and that both are responsible for the plasticity and short-term memory exhibited in our device (Figures 1, 3). In contrast, biosynapses rely on only ion channel dynamics for short-term plasticity.[38] Nonetheless, the increase in membrane area observed in our device can be likened to synthesis of additional α-amino-3-hydroxy-5-methyl-4-isoxazolepropionic acid (AMPA) receptors involved in short-term plasticity or to the creation of additional synapse area between nerves,[6] properties that could be further engineered to capture additional synaptic behaviors such as long-term potentiation.

Circuit Implementations and Simulations. The demonstrated properties of the biomolecular memristor (M1) suggest that it can be used as a synapse model to implement online learning functions, including spike-rate-dependent plasticity (SRDP) and STDP, as well as short- and long-term plasticity. We investigated these circuit implementations *via* simulations based on the described model. For short-term learning, M1 can be directly used as the synapse (Figure 5a), where the memory state information based on activation time creates a changing synaptic weight, similar to short-term plasticity in presynaptic neurons (Figure 5b). The weight increases as the input spikes occur with higher frequency (PPF), causing M1 to output higher current. When the input frequency decreases, the synapse returns to its original weight (PPD), due to its volatile nature. Simulations of the ideal device model show this functionality for a complete synaptic circuit (Figure 5a,b).

Our device, although volatile, can also be used to facilitate long-term learning (STDP), *via* PPF/PPD-like responses that update a nonvolatile metal-oxide memristor, M2 (Figure 5c). This paired scheme is akin to how AMPA receptors store memory but rely on NMDA receptors for learning. This configuration allowed the time difference between spikes from pre- and postneurons sent to M1 to adjust the current that can be sent to M2. We maintained the voltage drop across M1 *via* an amplifier that implemented a virtual ground on the input node, and thus the voltage-drop in the simulation was binary ±240 mV. When pre- and postspikes occurred, the state of M1, as well as its output current, was amplified and applied onto M2. At that time, the state of M1 was dependent on the time difference of the first input spike and the second input spike. Simulations using ideal device models show the resulting STDP in Figure 5d. This implementation of our biomolecular memristor requires simple spikes, either square or triangle waves, low power timing memory, due to the low voltage and currents of the memristor, and continuous-time asynchronous analogue weight updates. None of these features are currently implemented in state-of-the-art memristors, which require sophisticated and energy-consuming solid-state learning circuits.

CONCLUSION

We have presented a fundamentally different class of iononeuromorphic, soft, two-terminal biomolecular memristor that mimics the physical structure, switching mechanism, and ion transport of biosynapses. Voltage-dependent threshold switching and volatile memristive behavior were found through experiments and simulations to be governed by two voltage-dependent state variables, the areal density of alm channels and the increase in membrane area due to electrowetting, which dictate the total number of ion channels and, thus, the net conductance of the device. As a result, our device exhibits switching dynamics that are comparable to depolarizing pulses in actual nerve cells[49] and exhibits both short- and long-term plasticity such as PPF, PPD, SRDP, and, when paired with a nonvolatile memristor, STDP.

Compared to solid-state memristors, neuromorphic architectures based on stimuli-responsive biomolecules offer distinct advantages. Our self-assembled biomolecular memristors consume significantly less power (~0.1−10 nW), and they are relatively inexpensive and easily scalable *via* droplet-based printing[52] or microfluidic methods.[45] Further, circuity based on stimuli-responsive ion channels offers the possibility for adaptive learning and memory, as well as sensing, of many types of physical and chemical stimulations, possibly even at the same time and in the same membrane. Thus, the results presented here forecast an alternative paradigm for neuromorphic hardware using materials that could be integrated into synthetic multifunctional structures and interfaced with biological tissues to provide adaptive sensing, signal processing, smart edge computing, and memory.

MATERIALS AND METHODS

Preparation of Lipid and Peptide Solutions. The aqueous droplets consist of a suspension of phospholipid vesicles, salt, and a buffering agent in highly pure deionized water. Lipid vesicles are prepared and stored as described in various previously published articles (DPhPC[34] and BTLE[53]). The solutions contain 2 mg/mL DPhPC or BTLE liposomes in 500 mM potassium chloride (KCl, Sigma) and 10 mM 3-(N-morpholino)propanesulfonic acid (MOPS, Sigma) buffered with sodium hydroxide to a pH of 7. Agarose (Sigma) hydrogel (2% (w/v)) is prepared in the same electrolyte. A stock solution of 0.1% w/v alamethicin peptides (A.G. Scientific) in ethanol (Sigma) is diluted in the lipid vesicle solutions to yield final concentrations of 1 μM. The oil surrounding the droplets is hexadecane (99%, Sigma).

Formation of the Lipid Membrane. Droplet-based membranes are assembled between two aqueous droplets suspended from wire-type electrodes in an oil-filled, transparent reservoir, as described elsewhere.[46] Each 200 nL droplet is pipetted directly onto the tips of agarose-coated electrodes submerged in oil. The electrodes are silver/silver-chloride (Ag/AgCl) electrodes made from 150 μm of silver wire (Goodfellow), which have ball-ends to facilitate droplet holding. The oil reservoir is centered on an Olympus IX50 inverted microscope. A lipid monolayer self-assembles at the surface of each within minutes of their placement in oil. BTLE requires warming the oil to 50 °C to achieve sufficient monolayer formation.[53] A lipid bilayer forms spontaneously after lipid-coated droplets are placed into contact. While DPhPC membranes can be assembled and used at either room temperature (RT ≈ 20 °C) or 50 °C, BTLE membranes were found to exhibit greater stability and higher electrical resistance at RT. Therefore, we excluded measurements of alm−BTLE memristors at 50 °C.

Electrical Measurements. Current measurements were made using an Axopatch 200B patch clamp amplifier and Digidata 1440 data acquisition system (Molecular Devices). To reduce electrical noise, the experimental setup was placed within a grounded Faraday cage, where RMS noise was around 0.55 pA. We used a custom LabVIEW VI and NI four-channel analogue output module (NI 9263) as well as a Hewlett-Packard 3314A function generator to generate the necessary voltage waveforms. Outputs from these sources were routed to the headstage (Axopatch 200B) *via* the external input on the amplifier.

To confirm membrane formation and measure bilayer capacitance, we applied a 10 mV, 10 Hz triangular voltage waveform to the device and recorded the induced capacitive current, as previously described.[34] We performed cyclic voltammetry scans at various sweep rates to generate the I−V relationships and to determine voltage thresholds. The I−V loops presented in Figure 1 are obtained after subtracting residual capacitive current resulting from the lipid membrane, as described by Okazaki *et al.*[51] Voltage pulses and pulse waves are used to study the switching characteristics of the biomolecular memristors as well as PPF and PPD responses.

Simulations of switching mechanisms and circuit implementations. We simulated the switching mechanisms of our biomolecular memristor using the described model that includes equations of state for both alm pore formation (eq 2) and electrowetting of the membrane (eq 3). To do so, we first obtained estimates of the parameters in these state equations. Since EW is independent from alm insertion, we determined values of τ_{ew} and α for each membrane case by fitting numerical solutions of eq 3 to the measured change in membrane area during voltage sweeps (Supplementary Figure S10). Table S1 lists values of the EW parameters obtained in this manner. We then used these values with the measured relaxation time constants ($\tau_r \approx \tau_0$, Table 1) in a second fitting routine in which we estimated the parameters for alm insertion by fitting numerical solutions of eq 2 to the I−V responses given in Figure 1. Tables S2−S4 list values of V_τ, N_0, and V_e obtained for each case, and simulated I−V responses using these values are plotted in Supplementary Figure S6. Fitting routines to extract EW (Table S1) and alm parameters (Table S2−S4) were obtained using nonlinear minimization routines in MATLAB. Once these values were determined, they were fixed in subsequent simulations of device response to voltage sweeps and pulse waves.

Testing the device as a circuit component was performed *via* an ideal simulation in SPICE. Circuit components were implemented in Verilog-A. The model of the biomolecular memristor (M1) used the equations describing channel formation and electrowetting to calculate the changing resistance. The amplifier block takes the current through the device and outputs voltages that are above the switching threshold of the ideal memristor model used. The memristor (M2) model uses a linear relationship between the percentage change in resistance and the above-threshold voltage. The model is an ideal symmetric bipolar memristor. Ideal voltage sources in the SPICE simulation are used to stimulate the device.

ASSOCIATED CONTENT

Supporting Information

The Supporting Information is available free of charge on the ACS Publications website at DOI: 10.1021/acsnano.8b01282.

> Detailed description of the experimental setup, full mathematical derivations of the state equations, simulation results, and experimental results (PDF)

AUTHOR INFORMATION

Corresponding Authors

*(C. Patrick Collier) Phone: 865-576-3638. E-mail: colliercp@ornl.gov.
*(Stephen A. Sarles) Phone: 865-974-3488. E-mail: ssarles@utk.edu.

ORCID

Joseph S. Najem: 0000-0001-9687-886X
Graham J. Taylor: 0000-0001-8833-7705
Alex Belianinov: 0000-0002-3975-4112

Author Contributions

J.S.N., S.A.S., G.J.T., and C.P.C. designed experiments. J.S.N. performed experiments with inputs from G.J.T., S.A.S., R.J.W., and C.P.C. J.S.N. analyzed the experimental data. J.S.N., G.J.T., and S.A.S. developed mathematical models. G.J.T. developed LabVIEW software for stimulus generation and performed model simulations with inputs from J.S.N. and S.A.S. G.J.T. and J.S.N. analyzed simulation results. R.J.W., M.S.H., C.D.S., and G.S.R. designed circuit implementations and performed circuit simulations. J.S.N., S.A.S., C.P.C., A.B., R.J.W., and M.S.H. wrote the paper. J.S.N. prepared figures and Supporting Information. S.A.S., C.P.C., J.S.N., A.B., and G.S.R. conceived the concept. C.P.C. and S.A.S. planned and supervised the project. All discussed the results and implications and commented on the manuscript at all stages.

Notes

The authors declare no competing financial interest.

ACKNOWLEDGMENTS

Financial support was provided by the National Science Foundation Grant NSF ECCS-1631472. Research for G.J.T., C.D.S., A.B., and C.P.C. was partially sponsored by the Laboratory Directed Research and Development Program of Oak Ridge National Laboratory, managed by UT-Battelle, LLC, for the U.S. Department of Energy. A portion of this research was conducted at the Center for Nanophase Materials Sciences, which is a DOE Office of Science User Facility. The graphics in Figure 1a and Figure S2 were modified from Servier Medical Art (http://smart.servier.com), licensed under a Creative Common Attribution 3.0 Generic License.

REFERENCES

(1) Merolla, P. A.; Arthur, J. V.; Alvarez-Icaza, R.; Cassidy, A. S.; Sawada, J.; Akopyan, F.; Jackson, B. L.; Imam, N.; Guo, C.; Nakamura, Y. A Million Spiking-Neuron Integrated Circuit with a Scalable Communication Network and Interface. *Science* **2014**, *345*, 668−673.

(2) Benjamin, B. V.; Gao, P.; McQuinn, E.; Choudhary, S.; Chandrasekaran, A. R.; Bussat, J.-M.; Alvarez-Icaza, R.; Arthur, J. V.; Merolla, P. A.; Boahen, K. Neurogrid: A Mixed-Analog-Digital Multichip System for Large-Scale Neural Simulations. *Proc. IEEE* **2014**, *102*, 699−716.

(3) Scholze, S.; Eisenreich, H.; Höppner, S.; Ellguth, G.; Henker, S.; Ander, M.; Hänzsche, S.; Partzsch, J.; Mayr, C.; Schüffny, R. A 32gbit/

S Communication Soc for a Waferscale Neuromorphic System. *Integration* **2012**, *45*, 61−75.

(4) Furber, S. B.; Galluppi, F.; Temple, S.; Plana, L. A. The Spinnaker Project. *Proc. IEEE* **2014**, *102*, 652−665.

(5) Mayford, M.; Siegelbaum, S. A.; Kandel, E. R. Synapses and Memory Storage. *Cold Spring Harbor Perspect. Biol.* **2012**, *4*, a005751.

(6) Dan, Y.; Poo, M.-M. Spike Timing-Dependent Plasticity: From Synapse to Perception. *Physiol. Rev.* **2006**, *86*, 1033−1048.

(7) van den Heuvel, M. P.; Stam, C. J.; Kahn, R. S.; Pol, H. E. H. Efficiency of Functional Brain Networks and Intellectual Performance. *J. Neurosci.* **2009**, *29*, 7619−7624.

(8) Mead, C. Neuromorphic Electronic Systems. *Proc. IEEE* **1990**, *78*, 1629−1636.

(9) Diorio, C.; Hasler, P.; Minch, A.; Mead, C. A. A Single-Transistor Silicon Synapse. *IEEE Trans. Electron Devices* **1996**, *43*, 1972−1980.

(10) Strukov, D. B.; Snider, G. S.; Stewart, D. R.; Williams, R. S. The Missing Memristor Found. *Nature* **2008**, *453*, 80−83.

(11) Prodromakis, T.; Toumazou, C.; Chua, L. Two Centuries of Memristors. *Nat. Mater.* **2012**, *11*, 478.

(12) Jo, S. H.; Chang, T.; Ebong, I.; Bhadviya, B. B.; Mazumder, P.; Lu, W. Nanoscale Memristor Device as Synapse in Neuromorphic Systems. *Nano Lett.* **2010**, *10*, 1297−1301.

(13) Prezioso, M.; Merrikh-Bayat, F.; Hoskins, B.; Adam, G.; Likharev, K. K.; Strukov, D. B. Training and Operation of an Integrated Neuromorphic Network Based on Metal-Oxide Memristors. *Nature* **2015**, *521*, 61−64.

(14) Sheridan, P. M.; Cai, F.; Du, C.; Ma, W.; Zhang, Z.; Lu, W. D. Sparse Coding with Memristor Networks. *Nat. Nanotechnol.* **2017**, *12*, 784.

(15) Chua, L. Memristor-the Missing Circuit Element. *IEEE Trans. Circuit Theory* **1971**, *18*, 507−519.

(16) Williams, R. S. How We Found the Missing Memristor. *IEEE Spectrum* **2008**, *45*, 2810.1109/MSPEC.2008.4687366.

(17) Kwon, D.-H.; Kim, K. M.; Jang, J. H.; Jeon, J. M.; Lee, M. H.; Kim, G. H.; Li, X.-S.; Park, G.-S.; Lee, B.; Han, S. Atomic Structure of Conducting Nanofilaments in Tio2 Resistive Switching Memory. *Nat. Nanotechnol.* **2010**, *5*, 148−153.

(18) Wedig, A.; Luebben, M.; Cho, D.-Y.; Moors, M.; Skaja, K.; Rana, V.; Hasegawa, T.; Adepalli, K. K.; Yildiz, B.; Waser, R. Nanoscale Cation Motion in Taox, Hfox and Tiox Memristive Systems. *Nat. Nanotechnol.* **2016**, *11*, 67−74.

(19) Kim, S.; Du, C.; Sheridan, P.; Ma, W.; Choi, S.; Lu, W. D. Experimental Demonstration of a Second-Order Memristor and Its Ability to Biorealistically Implement Synaptic Plasticity. *Nano Lett.* **2015**, *15*, 2203−2211.

(20) Du, C.; Ma, W.; Chang, T.; Sheridan, P.; Lu, W. D. Biorealistic Implementation of Synaptic Functions with Oxide Memristors through Internal Ionic Dynamics. *Adv. Funct. Mater.* **2015**, *25*, 4290−4299.

(21) Wang, Z.; Joshi, S.; Savel'ev, S. E.; Jiang, H.; Midya, R.; Lin, P.; Hu, M.; Ge, N.; Strachan, J. P.; Li, Z. Memristors with Diffusive Dynamics as Synaptic Emulators for Neuromorphic Computing. *Nat. Mater.* **2017**, *16*, 101−108.

(22) Wang, Z.; Joshi, S.; Savel'ev, S.; Song, W.; Midya, R.; Li, Y.; Rao, M.; Yan, P.; Asapu, S.; Zhuo, Y. Fully Memristive Neural Networks for Pattern Classification with Unsupervised Learning. *Nat. Electron.* **2018**, *1*, 137.

(23) Berzina, T.; Smerieri, A.; Bernabò, M.; Pucci, A.; Ruggeri, G.; Erokhin, V.; Fontana, M. Optimization of an Organic Memristor as an Adaptive Memory Element. *J. Appl. Phys.* **2009**, *105*, 124515.

(24) Chen, Y.; Liu, G.; Wang, C.; Zhang, W.; Li, R.-W.; Wang, L. Polymer Memristor for Information Storage and Neuromorphic Applications. *Mater. Horiz.* **2014**, *1*, 489−506.

(25) van de Burgt, Y.; Lubberman, E.; Fuller, E. J.; Keene, S. T.; Faria, G. C.; Agarwal, S.; Marinella, M. J.; Talin, A. A.; Salleo, A. A Non-Volatile Organic Electrochemical Device as a Low-Voltage Artificial Synapse for Neuromorphic Computing. *Nat. Mater.* **2017**, *16*, 414−418.

(26) Chanthbouala, A.; Garcia, V.; Cherifi, R. O.; Bouzehouane, K.; Fusil, S.; Moya, X.; Xavier, S.; Yamada, H.; Deranlot, C.; Mathur, N. D. A Ferroelectric Memristor. *arXiv preprint, arXiv:1206.3397*, 2012.

(27) Kim, D.; Lu, H.; Ryu, S.; Bark, C.-W.; Eom, C.-B.; Tsymbal, E.; Gruverman, A. Ferroelectric Tunnel Memristor. *Nano Lett.* **2012**, *12*, 5697−5702.

(28) Liu, D.; Cheng, H.; Zhu, X.; Wang, G.; Wang, N. Analog Memristors Based on Thickening/Thinning of Ag Nanofilaments in Amorphous Manganite Thin Films. *ACS Appl. Mater. Interfaces* **2013**, *5*, 11258−11264.

(29) Liu, D.; Zhang, C.; Wang, G.; Shao, Z.; Zhu, X.; Wang, N.; Cheng, H. Nanoscale Electrochemical Metallization Memories Based on Amorphous (La, Sr) Mno3 Using Ultrathin Porous Alumina Masks. *J. Phys. D: Appl. Phys.* **2014**, *47*, 085108.

(30) Wang, X.; Chen, Y.; Xi, H.; Li, H.; Dimitrov, D. Spintronic Memristor through Spin-Torque-Induced Magnetization Motion. *IEEE Electron Device Lett.* **2009**, *30*, 294−297.

(31) Waldrop, M. M. The Chips Are Down for Moore's Law. *Nature* **2016**, *530*, 144−147.

(32) Li, C.; Hu, M.; Li, Y.; Jiang, H.; Ge, N.; Montgomery, E.; Zhang, J.; Song, W.; Dávila, N.; Graves, C. E.; Li, Z.; Strachan, J. P.; Lin, P.; Wang, Z.; Barnell, M.; Wu, Q.; Williams, R. S.; Yang, J. J.; Xia, Q. Analogue Signal and Image Processing with Large Memristor Crossbars. *Nat. Electron.* **2018**, *1*, 52−59.

(33) Sarles, S. A.; Leo, D. J. Regulated Attachment Method for Reconstituting Lipid Bilayers of Prescribed Size within Flexible Substrates. *Anal. Chem.* **2010**, *82*, 959−66.

(34) Taylor, G. J.; Venkatesan, G. A.; Collier, C. P.; Sarles, S. A. Direct *in Situ* Measurement of Specific Capacitance, Monolayer Tension, and Bilayer Tension in a Droplet Interface Bilayer. *Soft Matter* **2015**, *11*, 7592−7605.

(35) Cafiso, D. Alamethicin: A Peptide Model for Voltage Gating and Protein-Membrane Interactions. *Annu. Rev. Biophys. Biomol. Struct.* **1994**, *23*, 141−165.

(36) Chua, L. If It's Pinched It'sa Memristor. *Semicond. Sci. Technol.* **2014**, *29*, 104001.

(37) Chua, L.; Sbitnev, V.; Kim, H. Hodgkin−Huxley Axon Is Made of Memristors. *Int. J. Bifurcation Chaos Appl. Sci. Eng.* **2012**, *22*, 1230011.

(38) Zucker, R. S.; Regehr, W. G. Short-Term Synaptic Plasticity. *Annu. Rev. Physiol.* **2002**, *64*, 355−405.

(39) Kim, K.; Chen, C. L.; Truong, Q.; Shen, A. M.; Chen, Y. A Carbon Nanotube Synapse with Dynamic Logic and Learning. *Adv. Mater.* **2013**, *25*, 1693−1698.

(40) Sarwar, S. S.; Saqueb, S. A. N.; Quaiyum, F.; Rashid, A. H.-U. Memristor-Based Nonvolatile Random Access Memory: Hybrid Architecture for Low Power Compact Memory Design. *IEEE Access* **2013**, *1*, 29−34.

(41) Andersson, M.; Jackman, J.; Wilson, D.; Jarvoll, P.; Alfredsson, V.; Okeyo, G.; Duran, R. Vesicle and Bilayer Formation of Diphytanoylphosphatidylcholine (Dphpc) and Diphytanoylphosphatidylethanolamine (Dphpe) Mixtures and Their Bilayers' Electrical Stability. *Colloids Surf., B* **2011**, *82*, 550−561.

(42) Lee, J.; Kim, Y. H.; Arce, F.; Gillman, A. L.; Jang, H.; Kagan, B. L.; Nussinov, R.; Yang, J.; Lal, R. Amyloid B Ion Channels in a Membrane Comprising Brain Total Lipid Extracts. *ACS Chem. Neurosci.* **2017**, *8*, 1348.

(43) Bibette, J.; Calderon, F. L.; Poulin, P. Emulsions: Basic Principles. *Rep. Prog. Phys.* **1999**, *62*, 969.

(44) Ribrault, C.; Sekimoto, K.; Triller, A. From the Stochasticity of Molecular Processes to the Variability of Synaptic Transmission. *Nat. Rev. Neurosci.* **2011**, *12*, 375−388.

(45) Nguyen, M.-A.; Srijanto, B.; Collier, C. P.; Retterer, S. T.; Sarles, S. A. Hydrodynamic Trapping for Rapid Assembly and *in Situ* Electrical Characterization of Droplet Interface Bilayer Arrays. *Lab Chip* **2016**, *16*, 3576−3588.

(46) Taylor, G. J.; Sarles, S. A. Heating-Enabled Formation of Droplet Interface Bilayers Using Escherichia Coli Total Lipid Extract. *Langmuir* **2015**, *31*, 325−337.

(47) Krnjević, K. Chemical Nature of Synaptic Transmission in Vertebrates. *Physiol. Rev.* **1974**, *54*, 418−540.

(48) Lester, R. A.; Clements, J. D.; Westbrook, G. L.; Jahr, C. E. Channel Kinetics Determine the Time Course of Nmda Receptor-Mediated Synaptic Currents. *Nature* **1990**, *346*, 565−567.

(49) Sheng, J.; He, L.; Zheng, H.; Xue, L.; Luo, F.; Shin, W.; Sun, T.; Kuner, T.; Yue, D. T.; Wu, L.-G. Calcium-Channel Number Critically Influences Synaptic Strength and Plasticity at the Active Zone. *Nat. Neurosci.* **2012**, *15*, 998−1006.

(50) Stevens, C. F.; Wang, Y. Facilitation and Depression at Single Central Synapses. *Neuron* **1995**, *14*, 795−802.

(51) Okazaki, T.; Sakoh, M.; Nagaoka, Y.; Asami, K. Ion Channels of Alamethicin Dimer N-Terminally Linked by Disulfide Bond. *Biophys. J.* **2003**, *85*, 267−273.

(52) Villar, G.; Graham, A. D.; Bayley, H. A Tissue-Like Printed Material. *Science* **2013**, *340*, 48−52.

(53) Taylor, G. J.; Heberle, F. A.; Seinfeld, J. S.; Katsaras, J.; Collier, C. P.; Sarles, S. A. Capacitive Detection of Low-Enthalpy, Higher-Order Phase Transitions in Synthetic and Natural Composition Lipid Membranes. *Langmuir* **2017**, *33*, 10016−10026.